Accurate Spectrum Map Construction Using An Intelligent Frequency-Spatial Reasoning Approach

Chenyue Wang[§], Yuhang Wu[§], Fuhui Zhou[§], Qihui Wu[§], Chao Dong[§], and Kai-Kit Wong[†]
[§]Nanjing University of Aeronautics and Astronautics, Nanjing, China,
[†]University College London, London, UK.
Email: *cheyne@nuaa.edu.cn, may_wyh@nuaa.edu.cn, zhoufuhui@ieee.org, wuqihui@nuaa.edu.cn, dch@nuaa.edu.cn, kai-kit.wong@ucl.ac.uk*

***Abstract*—Spectrum map is of crucial importance for realizing efficient spectrum management in the sixth-generation (6G) wireless communication networks. However, the existing spectrum map construction schemes mainly depend on spatial interpolation and cannot construct the spectrum map when the measurement data of the target frequency are not obtained. In order to overcome this challenge, an accurate spectrum map construction scheme is proposed by using an intelligent frequency-spatial reasoning approach. The frequency correlation among different spectrum maps at different frequencies is fully exploited to construct the highly accurate spectrum maps of the frequencies without spectrum data. A novel autoencoder adapting to the three-dimensional (3D) spectrum data is proposed. Simulation results demonstrate that our proposed scheme is superior to the benchmark schemes in terms of the construction accuracy. Moreover, it is shown that our proposed autoencoder network has a fast convergence speed.**

***Index Terms*—Spectrum map, frequency correlation, frequency-spatial reasoning, autoencoder.**

I. Introduction

With the proliferation of intelligent terminals and the emergence of diverse ultra-wideband services, the spectrum scarcity and low utilization problems have been the major challenges for the sixth-generation (6G) wireless communication networks [1]. In order to tackle those challenges, intelligent spectrum management based on spectrum map was envisioned to be promising [1], [2]. Spectrum map is the projection of the received signal strength to the corresponding geographical coordinates in a region of interest for characterizing the spatial distribution of the received signal strength. It can provide the occupation and utilization situation of the spectrum resources and the activity distribution of the signal sources in an electromagnetic environment [1], [3]. Thus, how to accurately construct spectrum map is of crucial importance, and has received an increasing attention from both academia and industry.

The related works can be mainly categorized into the spatial-correlation-based schemes [1]-[4], [6]-[12] and the joint frequency-spatial-correlation-based schemes [5], [13]-[15]. They construct the spectrum map based on the correlation among spectrum data. The spatial-correlation-based schemes mainly have the model-based methods and the crowdsourcing-based methods [2]. The model-based methods generally rely on the priori assumptions of the propagation environments [1]-[4]. The accuracy of the spectrum maps achieved by using the model-based methods was poor due to the lack of flexibilities in the radio propagation. In contrast, the crowdsourcing-based methods constructed the spectrum maps more accurately via regression techniques or machine learning [5], such as matrix recovery [6], Kriging interpolation [7], the inverse distance weighted (IDW) interpolation [8], kernel-based learning [9], [10] and some data-driven methods proposed to further improve the accuracy [11], [12]. However, the spatial-correlation-based schemes only use spatial interpolation and cannot obtain the spectrum maps when there is no signal information about the target frequency.

Recently, the joint frequency-spatial-correlation-based schemes were proposed to tackle the above-mentioned problem by jointly considering the frequency and spatial correlation [5], [13]-[15]. Among the state-of-the-art works, the authors in [13] mentioned the concept of a spectrum map structure across different frequencies. However, they claimed that the propagation phenomena were similar at the neighbouring frequencies and the structure was directly separated across frequencies into various single-frequency spectrum maps, which ignored their frequency fading difference. The authors in [14] considered the spectrum map problem over several frequencies while the interfrequency relationship was not considered. Besides, a joint space-frequency interpolation scheme was proposed in [5] and [15]. Nevertheless, they simply used the values obtained over other frequencies as those over the frequency without signal information. In this case, the accuracy of the spectrum map is still not high, especially when the spectrum data of the target frequency are not obtained.

Note that the above-mentioned joint frequency-spatial-correlation-based works ignored the interfrequency fading difference during the radio propagation and simply used the frequency correlation, which limits the construction accuracy. Thus, it is infeasible for them to accurately construct the spectrum maps when the measurement data of the target frequency are not obtained. In practice, it is impossible that there are always available measurement data over the frequencies of interest since the amount of the measurement data is extremely large and the deployment cost of the sensors is

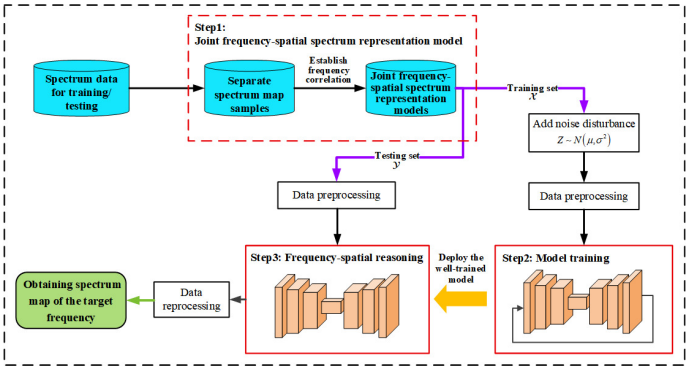

Fig. 1: The overview of our propsoed scheme.

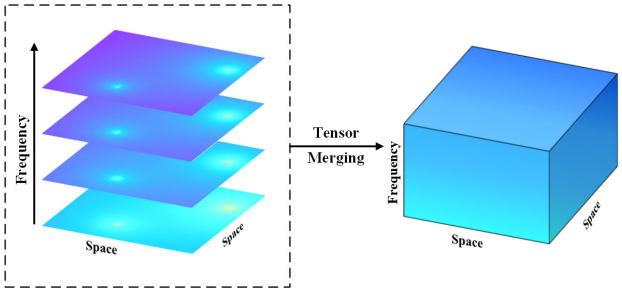

Fig. 2: The illustration of the frequency correlation establishing.

unaffordable when all frequencies within an ultra-wideband are considered. Moreover, more and more high frequency bands are licensed to be used for meeting the user connectivity and high data rate frequency. In this case, the measurement data of many frequencies in an ultra-wide frequency band may be not collected, which results in a significant challenge for accurately constructing spectrum map. Thus, it is practical and important to study how to accurately construct the spectrum maps of the target frequencies when their spectrum data are not obtained.

In this paper, in order to tackle the above-mentioned challenge and accurately construct spectrum map, considering the fact that the radio fading phenomena are different among various frequencies, an accurate spectrum map construction scheme is proposed by using an intelligent frequency-spatial reasoning approach. The frequency correlation among different spectrum maps at different frequencies is completely exploited to reason and estimate the target spectrum map by using our proposed novel autoencoder. Simulation results demonstrate that our proposed scheme can obtain the highly accurate spectrum maps of the frequencies without available spectrum data compared with the benchmark schemes. It is also shown that our proposed autoencoder network has a fast convergence speed, which benefits for the practical implementation.

The remainder of this paper is organized as follows. Section II formulates the spectrum map construction problem and Section III proposes our novel spectrum map construction scheme. In Section IV, simulation results are given. The paper is concluded in Section V.

II. Problem Formulation

A general scenario is considered that M transmitters are arbitrarily located in a target region of size $W \times W$ m and transmit signals on $K+1$ frequencies. Let the finite signal frequency set be denoted as $\mathcal{F} = \{f_1, f_2, \cdots, f_K, f_{target}\}$. Note that the order in the set does not represent the numerical relationship among frequencies. The sensors are randomly deployed at the geographical locations in the region in order to collect the received signal information over various frequencies. Then, the received signal data collected by the sensors together with the related parameters, such as the received locations and the signal frequencies, are transmitted to a base station or a cloud computing platform. Those data are used to infer the spectrum information about the target frequency and construct a complete spectrum map.

In order to construct the spectrum map, the geographical region is first uniformly discretized into $N \times N$ grids by using the grid quantization method [13], with the grid interval Δd. Let $\boldsymbol{\chi}$ denote the discretized geographical region. Let the grid point $\boldsymbol{I} = (i,j)$, $i,j = 0,1,\cdots,N-1$ denote the actual geographical location $\boldsymbol{x}_{i,j} = ((i+0.5)\Delta d, (j+0.5)\Delta d)$. It is assumed that the signal strength in a grid is consistent with that at the corresponding grid point. This assumption is reasonable since the signal strength changes a little when the grid is not large [13].

The received signal strength at the frequency f_k of the grid $\boldsymbol{I} = (i,j)$ is defined as $P(f_k, \boldsymbol{x}_{i,j})$, $k = 1,2,\cdots,K$, $i,j = 0,1,\cdots,N-1$. Then, a sparse spectrum map at the frequency f_k consisting of finite measurement data is expressed as a two-order tensor $\tilde{\mathbf{P}}^k \in \mathbb{R}^{N\times N}$. If the grid represented by $\boldsymbol{I} = (i,j)$ includes a sensor, the (i,j)th element $\left[\tilde{\mathbf{P}}^k\right]_{i,j}$ is given by the measurement result; otherwise, let $\left[\tilde{\mathbf{P}}^k\right]_{i,j} = 0$, indicating that the spectrum data at the grid do not exist. When multiple sensors exist in the same grid, these measurements are averaged. Similarly, a true spectrum map at the frequency f_k is represented as a tensor $\mathbf{P}^k \in \mathbb{R}^{N\times N}$, where $\left[\mathbf{P}^k\right]_{i,j} = P(f_k, \boldsymbol{x}_{i,j})$. And an estimated spectrum map at the frequency f_k is represented as a tensor $\hat{\mathbf{P}}^k \in \mathbb{R}^{N\times N}$.

In this paper, a practical and important problem is considered. Specifically, when the signal information about the target frequency is not obtained, how to accurately construct the target spectrum map tensor, i.e., $\hat{\mathbf{P}}^{target} \in \mathbb{R}^{N\times N}$, is studied by using the obtained sparse spectrum map tensors of other frequencies, i.e., $\left\{\tilde{\mathbf{P}}^k \in \mathbb{R}^{N\times N}\right\}_{k=1}^{M}$.

III. Our Proposed Accurate Spectrum Map Construction Scheme

In this section, the overview of our proposed accurate spectrum map construction scheme including three steps is first presented. Then, the joint frequency-spatial spectrum representation model in the first step is stated. Finally, a novel

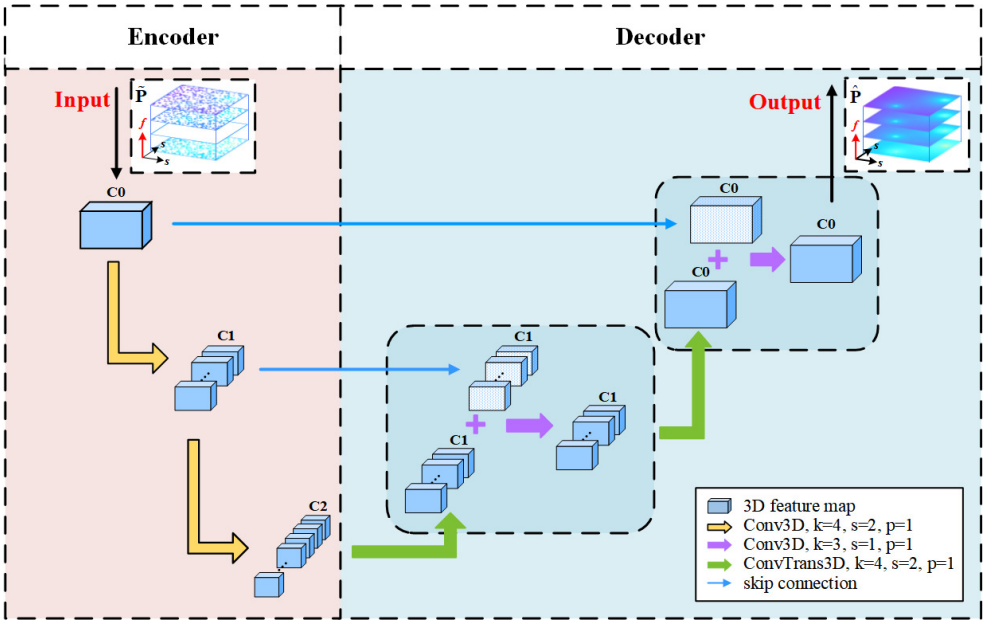

Fig. 3: Our proposed autoencoder structure. k, s and p respectively denote the size, stride and padding of the convolution layer, and C_0, C_1 and C_2 are the channel number of the output feature maps.

autoencoder structure used in the second and third steps is proposed.

A. The Overview of Our Proposed Scheme

For accurately constructing a spectrum map when the spectrum data of the target frequency are not obtained, the key is to fully exploit the frequency correlation among diverse spectrum maps. The overview of our proposed scheme is shown in Fig. 1. It has three steps stated as follows.

Firstly, the spectrum maps under the same radio propagation scenario while at different signal frequencies are stacked along the third dimension based on the numerical relationship among frequencies, as illustrated in Fig. 2. In this way, these single spectrum maps are effectively correlated over the frequency domain, and the frequency characteristics of the radio propagation phenomena can be learned in a three-dimensional (3D) structure. This operation is the crucial prerequisites for the following intelligent frequency-spatial reasoning about the data distribution of the spectrum maps.

Secondly, a method based on our novel autoencoder network is proposed to learn the frequency and spatial characteristics of the radio propagation phenomena, which benefits for inferring the target spectrum map. The novel autoencoder network is designed to use the sparse defective spectrum representation samples $\tilde{\mathbf{P}} \in \mathbb{R}^{(K+1)\times N\times N}$ as the input and output the complete spectrum representation results $\hat{\mathbf{P}} \in \mathbb{R}^{(K+1)\times N\times N}$. Let the mapping rule of the neural network be defined as a function $f_{\boldsymbol{\theta}}$, then, $f_{\boldsymbol{\theta}}\left(\tilde{\mathbf{P}}\right) = \hat{\mathbf{P}}$.

The model learns the characteristics of the radio propagation phenomena by training over the simulative training sets $\left\{\tilde{\mathbf{P}}, \mathbf{P}\right\}$. Specifically, the model is trained to learn the frequency fading characteristics in the frequency dimension and the spatial fading characteristics in the other geographical dimensions. The goal of training is to make the output of our proposed autoencoder network close to the true distribution of the spectrum data in the datasets. Therefore, the training objective is defined as

$$\min_{\boldsymbol{\theta}} \frac{1}{L\left(K+1\right)NN} \sum_{l=1}^{L} \left\| f_{\boldsymbol{\theta}}\left(\tilde{\mathbf{P}}_l\right) - \mathbf{P}_l \right\|_F^2, \tag{1}$$

where L represents the number of the training samples, l represents the lth training sample, and $(K+1)\times N\times N$ is the size of each 3D spectrum representation sample. $\|\cdot\|_F$ is the Frobenius norm of a tensor [13].

Thirdly, the well-trained model with reasoning capability is deployed to realize the intelligent frequency-spatial reasoning about the data distribution of the spectrum maps. Specifically, the finite sparse spectrum data obtained over other frequencies by measurement campaigns are sent to the well-trained model as the input for accurately inferring the complete spectrum representation tensor.

While the output of the network is the joint frequency-spatial spectrum representation model consisting of multiple frequencies. In order to obtain the spectrum map of the target frequency, the output of the network requires reprocessing. Specifically, the slice corresponding to the target frequency is searched and extracted from the joint spectrum representation model to obtain the target spectrum map $\hat{\mathbf{P}}^{target} \in \mathbb{R}^{N\times N}$.

B. Joint Frequency-Spatial Spectrum Representation Model and Problem Reformulation

Specifically, the $K+1$ sparse spectrum map tensors at different frequencies are stacked along the frequency dimension based on the order from the low frequency to the high

frequency, and merged into a 3D structure. Note that the spectrum map of the target frequency is a blank one without any measurement data, namely, $\tilde{\mathbf{P}}^{target}$ is a zero tensor, while the others are the sparse spectrum maps containing finite measurement data. Let a three-order tensor $\tilde{\mathbf{P}} \in \mathbb{R}^{(K+1)\times N\times N}$ denote the sparse 3D spectrum representation. Similarly, let a three-order tensor $\hat{\mathbf{P}} \in \mathbb{R}^{(K+1)\times N\times N}$ denote the estimated 3D spectrum representation and a three-order tensor $\mathbf{P} \in \mathbb{R}^{(K+1)\times N\times N}$ denote the true 3D spectrum representation. Through this operation, the separate spectrum maps are correlated over the frequency domain in the 3D spectrum representation model and the spectrum map construction problem is reformulatd as the one based on the 3D shape.

It is worth noting that our proposed 3D spectrum representation model is a joint frequency-spatial spectrum representation, which is very different from a conventional 3D spectrum map model considering only the single spatial domain. That is, the third dimension of our proposed 3D spectrum representation model is the frequency dimension, while that of a conventional one is the height dimension and is still in the geographical aspects.

C. Novel Low-Complexity Autoencoder Suitable for Three-Dimensional Data

The autoencoder neural network is a kind of deep neural networks based on a pixel-level semantic segmentation structure named U-Net [16]. Its structure is divided into two parts, namely, the contraction path (i.e., encoder $\varepsilon_{\boldsymbol{\theta}}$) and the expansion path (i.e., decoder $\delta_{\boldsymbol{\theta}}$). In this paper, a novel autoencoder based on the U-Net structure is proposed for the intelligent frequency-spatial reasoning by taking our proposed 3D spectrum representation samples as its input. Firstly, the encoder is implemented to extract the distribution characteristics of the samples both in the frequency and spatial dimensions, depending mainly on the improved 3D convolution layers. Then, the decoder is implemented to recover the complete 3D spectrum representation samples, depending mainly on the improved 3D transposed convolution layers. Our proposed autoencoder network structure is shown in Fig. 3 and its mapping function is expressed as

$$f_{\boldsymbol{\theta}}\left(\tilde{\mathbf{P}}\right) = \delta_{\boldsymbol{\theta}}\left(\varepsilon_{\boldsymbol{\theta}}\left(\tilde{\mathbf{P}}\right)\right), \tag{2}$$

where $\delta_{\boldsymbol{\theta}}$ denotes the decoder and $\varepsilon_{\boldsymbol{\theta}}$ denotes the encoder.

Noting that the conventional U-Net structure tailored to the 2D data processing is not respectably suitable for our proposed 3D data structure due to the inevitable problems arising from the excessive parameters of the 3D data. Specifically, both of the training complexity and the over-fitting risk increase with the number of data dimensions if the conventional U-Net structure is used. Therefore, a novel U-Net structure is designed for processing 3D data. The details of our proposed autoencoder structure are stated as follows.

1) The novel autoencoder network is composed of six layers. It greatly decreases the number of the neural network layers compared to the conventional U-Net deep neural network structure. The parameter load is alleviated and the training complexity is reduced accordingly by decreasing the depth of the neural network.
2) The core components of our network are the improved 3D convolution layer and 3D transposed convolution layer suitable for processing 3D data. The parameters of the convolution kernel are set as $k = 4$, $s = 2$ and $p = 1$, which are different from the common settings of a convolution layer, i.e., $k = 3$, $s = 1$ and $p = 1$. It is obvious that our convolution layer is capable of compressing the size of the feature maps while increasing the channel number. In this way, the layers routinely following the convolution operation are no longer required, such as the pooling and down-sampling layers. This design reduces the depth of the network and alleviates the training complexity consequently.
3) In order to avoid overfitting caused by overextracting the features of the datasets, the double-convolution-layer combination in the conventional U-Nets is replaced with a single convolution layer.
4) Finally, the decoder obtains the feature maps from the corresponding layers in the encoder and merges them in the channel dimension. The high-resolution feature maps from the encoder provide the decoder with more fine features and improve the construction capability of our network.

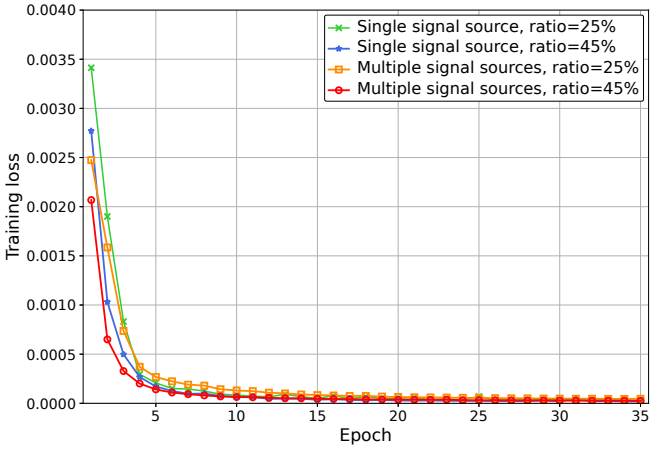

Fig. 4: The training loss curves of the proposed 3D-data-adapted autoencoder network in various circumstances.

IV. Simulation Results

In this section, the simulation details including the parameter settings and dataset generation are first presented. Then, the simulation results are given to demonstrate the superiority of our proposed scheme compared with the benchmark schemes.

A. Parameter Setting and Dataset Generation

The parameter settings are present as follows based on those used in [5] and [13]. $\boldsymbol{\chi}$ is a discretized square region

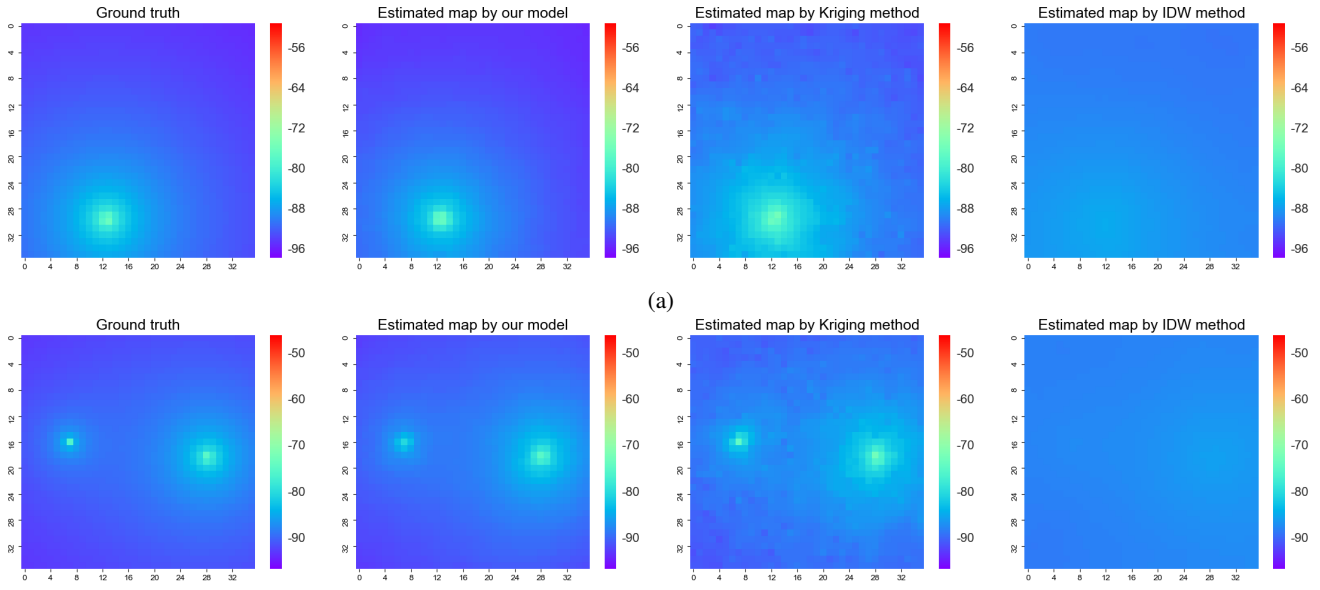

Fig. 5: The visualization results of the estimated spectrum maps under different schemes. (a) The results of a single-signal-source case; (b) The results of a double-signal-source case.

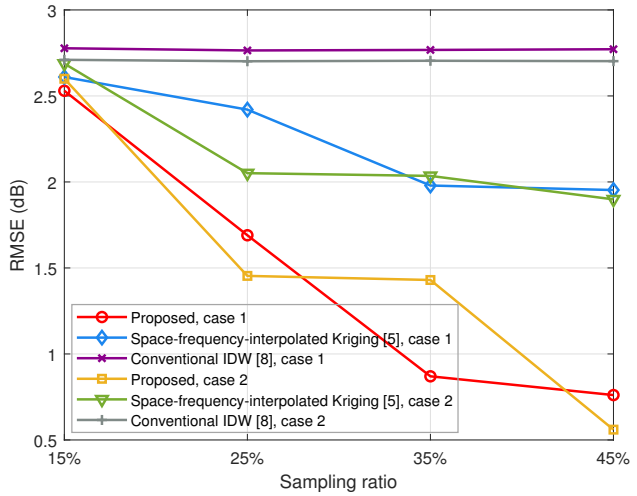

Fig. 6: The construction performance versus the sampling ratio under different schemes.

of 36×36 grids representing an actual geographical region of side 100 m. The propagation pass loss coefficients of the environment over the frequency and distance are 20 and 1, respectively. The transmitters are deployed randomly and the signal frequency set $\mathcal{F}$ is set to $\mathcal{F} = \{900, 1500, 1800, 2100\}$ MHz, of which any one can be set as a target frequency. Two cases are considered. One case has a single signal source while the other one has multiple signal sources. While the numbers of the sensors are determined by the sampling ratios range from 15% to 45% with a step of 10%, and the locations are randomly generated. For each setting, a separate dataset consisting of over 3×10^4 samples are generated according to our radio propagation model given as follows and divided into a training set and a testing set in the fixed proportion.

Remark 1: For the radio propagation model, it is considered that a transmitter sends a signal at the frequency f_k, and the large-scale fading during the propagation is taken into account since the effects of the small-scale fading can be averaged out when dealing with the average received signal strength [13]. Then, the received signal strength at the location $x_{i,j}$ from the transmitter is modeled as

$$P\left(f_k, \boldsymbol{x}_{i,j}\right) = P_{Tx} - n_f \log_{10}\left(f_k\right) - 10 n_d \log_{10}\left(d\right) - L_C, \tag{3}$$

where P_{Tx} represents the transmitting power of the signal source (dBm). n_f and n_d represent the path loss coefficients over the frequency and distance, respectively. L_C is the free-space propagation loss which remains constant over time. d is the distance between the transmitter and the receiver.

In order to show the measurement error in the actual measurement campaign, the additive zero-mean Gaussian noise is added to each simulative measurement as a random noise disturbance. It enables the model to extract the true distribution of the spectrum data from the 'dirty' defective data. In this case, the generalization ability of the model is improved.

Data preprocessing (i.e., data normalization) is carried out before feeding the datasets into our autoencoder network, for the sake of learning better the distribution characteristics of the samples and reaching more ideal results during the backward gradient propagation and model weight update. The received signal strength at each grid point is normalized as

$$P = \frac{P_0 - P_{\min}}{P_{\max} - P_{\min}}, \tag{4}$$

where $P_{\max}$ and $P_{\min}$ represent the maximum and minimum of the received signal strength in the datasets, respectively. Through data normalization, the inputs of our network are reshaped with one more channel. Thus, the dimensions of the inputs become $1 \times (K+1) \times N \times N$ and the value range is $[0, 1]$.

B. Performance Evaluation

The neural network is developed and trained in PyTorch platform by an Adam optimizer with an initial learning rate of 0.0005 for 35 epochs. The mini-batch training strategy is utilized. Whenever a batch of training is finished, a backward gradient propagation pass is conducted to update the trainable parameters of the network.

Fig. 4 shows the training loss curves of our proposed autoencoder network achieved under different numbers of sources with diverse sampling ratios. It is shown that our network has a fast convergence speed in all settings. Moreover, the training loss decreases to a very low level within 5 epochs and achieves convergence within 10 epochs in all settings. This demonstrates the efficiency of our proposed autoencoder network.

To intuitively compare the construction results of different schemes, Fig. 5 shows the visualization results of the spectrum maps obtained by our proposed scheme and those achieved by using different interpolation methods including the space-frequency-interpolated Kriging [5] and the inverse distance weighted (IDW) interpolation [8]. It is realized by mapping the normalized signal strength of each geographical grid to the corresponding color of a colorbar. Fig. 5(a) shows the results of a single-source scenario while Fig. 5(b) shows those of a double-source scenario, both presenting the true spectrum map, the spectrum map constructed by our proposed scheme, the space-frequency-interpolated Kriging and the IDW interpolation in sequence. It is obvious that our scheme outperforms the benchmark schemes in terms of the accuracy. Moreover, it can characterize the overall distribution of spectrum usage and the locations of the signal sources.

In order to further demonstrate the superiority of our proposed scheme, Fig. 6 compares the construction performance of our proposed scheme with those of the benchmark schemes. The abscissa and ordinate represent the sampling ratio ($\%$) and the construction error (dB), respectively. It can be observed that our scheme is significantly superior to the benchmark schemes. Taking the single-source scenario as an example, its construction error is about 2.53 dB at the 15% sampling ratio, which is about 3% lower than that of the space-frequency-interpolated Kriging method and 9% lower than that of the IDW interpolation method. And its construction error reaches about 0.76 dB at the 45% sampling ratio, which is approximately 61% lower than that of the space-frequency-interpolated Kriging method and 72% lower than that of the IDW interpolation method. Moreover, it is seen that the construction accuracy of our scheme increases with the sampling ratio. The reason is that the model is provided with more effective information from the spectrum data for learning the distribution when the datasets contain more sampling data.

V. Conclusion

An accurate spectrum map construction scheme was proposed by using an intelligent frequency-spatial reasoning approach. The frequency correlation among different spectrum maps at different frequencies was fully exploited to accurately estimate the spectrum maps of the frequencies without data samples. A novel autoencoder suitable for processing 3D data was proposed to learn and utilize the frequency and spatial characteristics of the radio propagation. Simulation results demonstrated the superiority of our proposed scheme in terms of the construction accuracy and the convergence speed of our network compared with the benchmark schemes.

References

[1] D. Lee, S. Kim, and G. B. Giannakis, "Channel gain cartography for cognitive radios leveraging low rank and sparsity," *IEEE Trans. Wireless Commun.*, vol. 16, no. 9, pp. 5953-5966, Sep. 2017.

[2] K. Sato and T. Fujii, "Kriging-based interference power constraint: integrated design of the radio environment map and transmission power," *IEEE Trans. Cogn. Commun. Netw.*, vol. 3, no. 1, pp. 13-25, Mar. 2017.

[3] D. Romero, D. Lee, and G. B. Giannakis, "Blind radio tomography," *IEEE Trans. Signal Process.*, vol. 66, no. 8, pp. 2055-2069, Apr. 2018.

[4] D. Lee, D. Berberidis, and G. B. Giannakis, "Adaptive bayesian radio tomography," *IEEE Trans. Signal Process.*, vol. 67, no. 8, pp. 1964-1977, Apr. 2019.

[5] K. Sato, K. Suto, K. Inage, K. Adachi, and T. Fujii, "Space-frequency-interpolated radio map," *IEEE Trans. Veh. Technol.*, vol. 70, no. 1, pp. 714-725, Jan. 2021.

[6] Y. Zhang and L. Ma, "Radio map crowdsourcing update method using sparse representation and low rank matrix recovery for WLAN indoor positioning system," *IEEE Wireless Commun. Lett.*, vol. 10, no. 6, pp. 1188-1191, Jun. 2021.

[7] D. Mao, W. Shao, Z. Qian, H. Xue, X. Lu, and H. Wu, "Constructing accurate radio environment maps with Kriging interpolation in cognitive radio networks," *Cross Strait Quad-Regional Radio Science and Wireless Technol. Conf.*, Jul. 2018.

[8] Z. El-friakh, A. M. Voicu, S. Shabani, L. Simić, and P. Mähönen, "Crowdsourced indoor Wi-Fi REMs: Does the spatial interpolation method matter?," *IEEE DySPAN 2018*, Seoul, Korea, Oct. 2018.

[9] D. Romero, S. Kim, G. B. Giannakis, and R. Lopez-Valcarce, "Learning power spectrum maps from quantized power measurements," *IEEE Trans. Signal Process.*, vol. 65, no. 10, pp. 2547-2560, May. 2017.

[10] Y. Xu, B. Zhang, X. Zhang, J. Hu, and D. Guo, "Radio environment map construction with Gaussian process and Kernel transformation," *Int. Conf. Commun, Image and Signal Process.*, Chengdu, China, Nov. 2021.

[11] K. Suto, S. Bannai, K. Sato, K. Inage, K. Adachi, and T. Fujii, "Image-driven spatial interpolation with deep learning for radio map construction," *IEEE Wireless Commun. Lett.*, vol. 10, no. 6, pp. 1222-1226, June 2021.

[12] J. Thrane, D. Zibar, and H. L. Christiansen, "Model-aided deep learning method for path loss prediction in mobile communication systems at 2.6 ghz," *IEEE Access*, vol. 8, pp. 7925-7936, Jan. 2020.

[13] Y. Teganya and D. Romero, "Deep completion autoencoders for radio map estimation," *IEEE Trans. Wireless Commun.*, vol. 21, no. 3, pp. 1710-1724, March 2022.

[14] S. Shrestha, X. Fu, and M. Hong, "Deep generative model learning for blind spectrum cartography with NMF-based radio map disaggregation," *IEEE Int. Conf. Acoustics, Speech and Signal Process.*, Toronto, Canada, June 2021.

[15] K. Sato, K. Inage, and T. Fujii, "Radio environment map construction with joint space-frequency interpolation," *ICAIIC 2020*, Fukuoka, Japan, Feb. 2020.

[16] M.-H. Sheu, S. M. S. Morsalin, S.-H. Wang, L.-K. Wei, S.-C. Hsia, and C.-Y. Chang, "FHI-Unet: faster heterogeneous images semantic segmentation design and edge AI implementation for visible and thermal images processing," *IEEE Access*, vol. 10, pp. 18596-18607, Feb. 2022.